Check for updates

View Article Online
View Journal

Sustainable Food Technology

Accepted Manuscript

This article can be cited before page numbers have been issued, to do this please use: J. Fujera, T. Homola, K. Siruckova Lonova, P. Kalousek, G. Arora, A. Artemenko, V. Prukner and M. Simek, *Sustainable Food Technol.*, 2026, DOI: 10.1039/D6FB00081A.

This is an Accepted Manuscript, which has been through the Royal Society of Chemistry peer review process and has been accepted for publication.

Accepted Manuscripts are published online shortly after acceptance, before technical editing, formatting and proof reading. Using this free service, authors can make their results available to the community, in citable form, before we publish the edited article. We will replace this Accepted Manuscript with the edited and formatted Advance Article as soon as it is available.

You can find more information about Accepted Manuscripts in the Information for Authors.

Please note that technical editing may introduce minor changes to the text and/or graphics, which may alter content. The journal's standard Terms & Conditions and the Ethical guidelines still apply. In no event shall the Royal Society of Chemistry be held responsible for any errors or omissions in this Accepted Manuscript or any consequences arising from the use of any information it contains.

ROYAL SOCIETY
OF CHEMISTRY

View Article Online
DOI: 10.1039/D6FB00081A

Sustainability spotlight

Traditional seed priming often relies on large volumes of water or synthetic chemical stimulants to break dormancy and ensure uniform crop establishment, which in industrial sectors like malting can be quite water intensive. This research uses Volume Dielectric Barrier Discharge (DBD) to modify the surface of barley seeds. By employing amplitude-modulated AC plasma microfilaments in simple dry air, a precise, targeted modification of the seed coat's chemistry from hydrophobic to hydrophilic was achieved. As a completely dry process, there is no contaminated aqueous runoff, simplifying the path toward zero liquid consumption in seed processing facilities. This approach to seed priming thus aligns with at least three UN Sustainable Development Goals, including SDG 2 (Zero Hunger), SDG 6 (Clean Water and Sanitation), and SDG 12 (Responsible Consumption and Production), underscoring its potential to advance innovative, resource-efficient, and environmentally responsible food processing.

Open Access Article. Published on 15 June 2026. Downloaded on 6/15/2026 11:33:03 PM.
This article is licensed under a Creative Commons Attribution 3.0 Unported Licence.

Sustainable Food Technology Accepted Manuscript

View Article Online
DOI: 10.1039/D6FB00081A

ARTICLE

Direct Volume DBD Plasma Treatment of Barley Seeds (*Hordeum vulgare*): Impact of Surface Functionalization on Germination and Root Development

Received 00th January 20xx,
Accepted 00th January 20xx

DOI: 10.1039/x0xx00000x

Jiří Fujera[a,d*], Tomáš Homola[a,d], Kamila Širůčková Lónová[b], Petr Kalousek[b], Garima Arora[a], Anna Artemenko[c], Václav Prukner[a], and Milan Šimek[a]

Cold atmospheric plasma (CAP) is an emerging, chemical-free technology with significant potential to enhance crop performance. This study investigates the impact of direct plasma treatment on barley (*Hordeum vulgare*) seeds using an amplitude-modulated AC dielectric barrier discharge (DBD) in dry synthetic air. By impinging plasma microfilaments directly onto the seed surface, we enabled precise dose estimation and optimization. Plasma microfilaments were generated by amplitude-modulated AC dielectric barrier discharge in dry synthetic air, and the treatment time ranged from 10 seconds to 5 minutes. After treatment, the barley seed surface was analyzed for morphological and chemical changes, as well as for imbibition and germination rates. X-ray photoelectron spectroscopy (XPS) and sessile drop methods revealed a distinct chemical transition from a hydrophobic state, dominated by C-C/C-H bonds, to a polar, oxygen-enriched hydrophilic surface. While these surface modifications accelerated water imbibition, this physical enhancement did not translate into a statistically significant increase in germination speed. This non-monotonic relationship suggests that while Volume DBD effectively tailors seed surface chemistry for improved hydration, the biological triggers for germination may require further optimization of plasma-induced signaling. These findings provide a fundamental framework for developing sustainable dry-priming protocols that minimize water and chemical use in the industrial malting and agricultural sectors.

Sustainability spotlight

Traditional seed priming often relies on large volumes of water or synthetic chemical stimulants to break dormancy and ensure uniform crop establishment, which in industrial sectors like malting can be quite water intensive. This research uses Volume Dielectric Barrier Discharge (DBD) to modify the surface of barley seeds. By employing amplitude-modulated AC plasma microfilaments in simple dry air, a precise, targeted modification of the seed coat's chemistry from hydrophobic to hydrophilic was achieved. As a completely dry process, there is no contaminated aqueous runoff, simplifying the path toward zero liquid consumption in seed processing facilities. This approach to seed priming thus aligns with at least three UN Sustainable Development Goals, including SDG 2 (Zero Hunger), SDG 6 (Clean Water and Sanitation), and SDG 12 (Responsible Consumption and Production), underscoring its potential to advance innovative, resource-efficient, and environmentally responsible food processing.

Introduction

Research into the use of cold plasma in the agri-food sector in recent years has generally focused on increasing productivity (reducing losses) while maintaining the quality of produce/food[1–8]. The effects of plasma, most often on plant seeds, have been studied at various levels, from (chemical and physical) changes to the seed coat (including microbial decontamination), through processes associated with germination and occurring within the seeds, to early seedling development and subsequent growth of developing plants (seed priming)[9–16]. For example, the low-pressure RF argon gas discharge treatment increased the safflower seed germination rate[17] and reduced the germination time. These effects were attributed to seed surface cleaning, etching (scarification), and chemical and physical modifications of the pericarp and hilum structure. Similarly, the cold plasma treatment increased the germination rate of oil-seed rape and seedlings' growth (including the lateral root number), increased superoxide dismutase (SOD) and catalase activities, and reduced lipid peroxidation (and malondialdehyde - MDA content) under drought stress[18]. A similar effect was reported in cold plasma-treated tomato seeds and seedlings[19]. On the other hand, cold plasma treatment of pea seeds[20] improved their growth, some photosynthetic parameters, nodulation, and nitrogen fixation, and thereby increased yield in plants cultivated under well-watered but not under drought conditions. The positive effect of plasma treatment was also found in other plants from the legume family. Cold plasma treatment

[a.] [1]*Institute of Plasma Physics of the Czech Acad Sci, Prague, Czech Republic*
[b.] [2]*Department of Plant Biology, Faculty of AgriSciences, Mendel University in Brno, Czech Republic*
[c.] [3]*Institute of Physics, Czech Academy of Sciences, Prague, Czech Republic*
[d.] [4]*Department of Plasma Physics and Technology, Faculty of Science, Masaryk University, Brno, Czech Republic*

† Footnotes relating to the title and/or authors should appear here.
Supplementary Information available: [details of any supplementary information available should be included here]. See DOI: 10.1039/x0xx00000x

Open Access Article. Published on 15 June 2026. Downloaded on 6/15/2026 11:33:03 PM.
This article is licensed under a Creative Commons Attribution 3.0 Unported Licence.

Sustainable Food Technology Accepted Manuscript

View Article Online
DOI: 10.1039/D5FB00081A

improved the water uptake in soybean seeds and stimulated the growth of the root system of seedlings, as well as increased seed reserve depletion and utilization efficiency[21].

Figure 1: Cross-section of a barley caryopsis: SE - central starchy endosperm, SA - subaleurone cells, AL – aleurone, T – testa, P – pericarp. Stained with Safranin O and Fast Green FCF.

Healthy and vital plants are the basis for food, feed, and seed production. Supporting seed germination and improving seedling vitality are the key factors for crop production in subsequent seasons. One of the most important crop groups is cereals (wheat, barley, oat, rye, rice, maize, etc.). Barley (*Hordeum vulgare*) is one of the four most important cereal crops in the world. Its kernels are important for the feed production and human food for their high content of health-promoting substances such as dietary fibre, β-glucans, lipids, proteins, minerals, phenolic compounds, and B-type and E-type vitamins[22,23]. No less important is the necessity of barley grain for malt production, which is an essential ingredient for brewing. [24]The microbiological purity of the raw material (barley kernels) and the evenness of grain germination, as well as the termination of the dormancy process, are therefore key to the malting process[24]. Plasma treatment of barley kernels could help improve the production of high-quality malt, as well as attain the development of more vital and stress-tolerant plants from the plasma-treated seeds.

Barley kernel anatomy, chemical composition of the seed coat and its impact on germination

The dispersal unit of the barley plant (*Hordeum vulgare L.*) is the kernel (*caryopses*), which is the dry fruit containing one seed with an embryo. The largest proportion of barley kernel volume (and weight) is nutrient-rich tissue, which consists of starchy endosperm and two to four aleurone layers[25]. Around the seed is the seed coat (*testa*), which is fused with the multilayered dead pericarp (Figure 1). The whole barley kernel is covered with hulls consisting of the outer (external) lemma and the inner (internal) palea[26]. Each of these parts consists of four different types of tissues: the outer epidermis, sclerenchyma with rigid lignin-rich cell walls, parenchyma with vascular bundles, and the inner epidermis[27]. For generative plant propagation, seed (in the case of barley, kernel) viability is crucial. Viability is manifested by germination and the subsequent development of seedlings under suitable exogenous and endogenous conditions. The first step in the germination process is the physical process of imbibition, which consists of the absorption of water by the seed; the second phase ends with the rupture of covering layers by roots (respectively in the case of monocotyledons, including barley, by coleorhiza)[28]. The third part of germination characterizes the early seedlings' development[29].

The permeability of the seed coat (in barley, influenced primarily by its chemical composition, more than by its thickness[30]) plays a crucial role in water uptake during the seed imbibition[29,31], during which water binds (is absorbed) to hydrophilic compounds in cell walls (polysaccharides as β-glucanes, proteins, etc.). The water taken up is further distributed along the decreasing water potential gradient[32]. During imbibition swelling, the kernel increases in volume, and its surface becomes smooth (Figure 2).

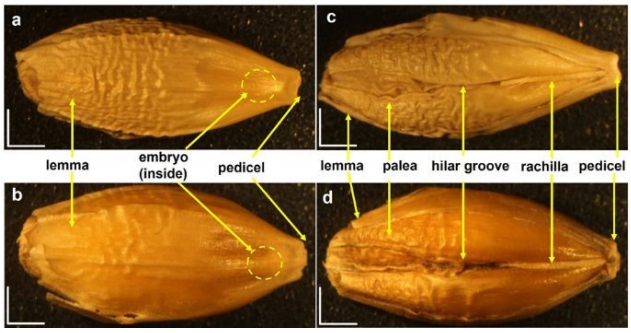

Figure 2: Dorsal (a, b) and ventral side (c, d) of dry (a, c) and imbibed (b, d) barley kernel after 1hour imbibition. The white lines represent a distance of 1 mm.

At the beginning of this phase, water intake is very intense (7.1% per hour), but then gradually decreases (1.2%), and subsequently rises to 5.2% per hour[28]. Then the other parts of the kernel are hydrated, hydrolytic enzymes are activated by gibberellic signal, and digest storage compounds (as the starch in endosperm and proteins in aleurone)[28,29]. Although water intake is essential for germination and related processes, excessive and uncontrolled water intake can lead to seed damage, reduce its viability, or cause solute leakage, which can also affect seedling development (imbibition injuries). On the other hand, the rate of seed water uptake can also be affected by seed viability and the integrity of the seed coats[32]. As was mentioned above, the uppermost covering part of the barley kernel is made up of two layers of the husk. These, lemma and palea, are composed of cells with suberin-rich cell walls[27]. Neitzel et al.[33], while investigating the physical and biochemical properties of barley husks, found that they contain a comparatively large amount of lignin and ash. Suberin and lignin are hydrophobic compounds[34,35] that could pose a chemical obstacle for imbibition. It was also reported that barley husks have a high microfibril angle (MFA) value, which is formed between the cellulose microfibrils and the fiber's longitudinal

Open Access Article. Published on 15 June 2026. Downloaded on 6/15/2026 11:33:03 PM.
This article is licensed under a Creative Commons Attribution 3.0 Unported Licence.

Sustainable Food Technology Accepted Manuscript

This journal is © The Royal Society of Chemistry 20xx

Please do not adjust margins

View Article Online
DOI: 10.1039/D6FB00045F

Open Access Article. Published on 15 June 2026. Downloaded on 6/15/2026 11:33:03 PM.
This article is licensed under a Creative Commons Attribution 3.0 Unported Licence.

Sustainable Food Technology Accepted Manuscript

axis. It indicates low mechanical resistance and, therefore, a possible higher susceptibility to damage[33], by, for example, plasma discharge. Mechanical or chemical surface disturbance could help to improve the water permeability of seed covering layers, but the enormous surface damage associated with rapid water uptake causes cell ruptures and leads to cell-solutes leaching[32]. The duration of the imbibition phase is closely related to the seed condition and the ambient condition, such as temperature, water viscosity, or osmolarity. However, in the case of barley kernels, the imbibition time is reported to be approximately 2.5 hours (in a broader sense, 10 hours)[28]. This phase is followed by germination, during which the key enzymes are gradually activated. All germination stages are accompanied and influenced by changing levels of ROS (reactive oxygen species) and RNS (reactive nitrogen species). They function as important signaling molecules and play a significant role in regulating growth and development. On the other hand, their higher concentrations cause oxidative damage of proteins, lipids, and nucleic acids[36]. The role of ROS as signaling molecules is

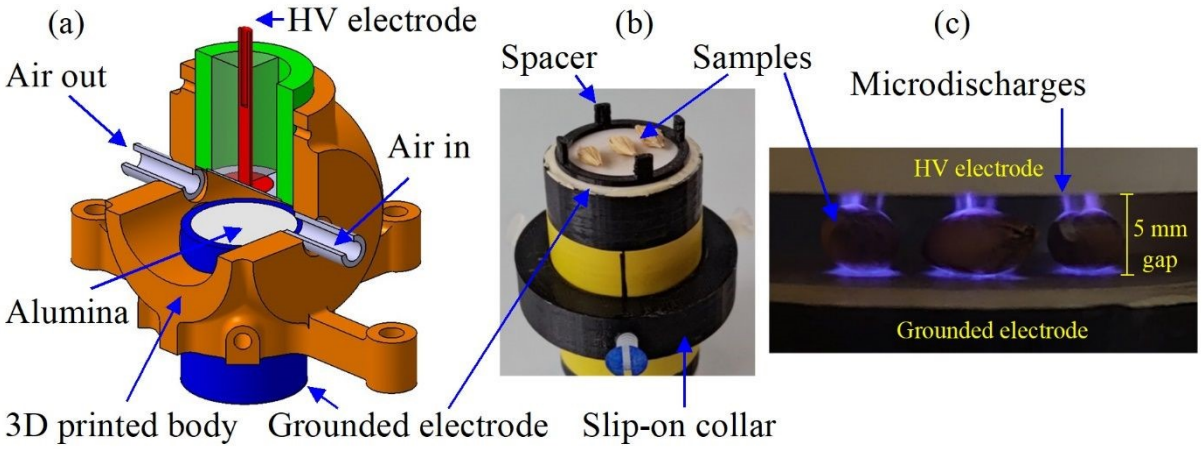

Figure 3: Experimental setup. (a) simplified sketch of the used 3D-printed volume DBD reactor, b) a photograph of the sample holder with a spacer for the precise definition of the DBD gap, c) an image of *Hordeum vulgare* seeds in the discharge.

important mainly in the second phase of germination, when metabolic processes associated with changes in phytohormone levels and activation of hydrolytic enzymes are activated[29,37]. It has also been reported that in this middle stage of germination, nitric oxide (NO) endogenous levels increase in barley kernels[38]. RNS are produced in an increased amount at this stage of germination due to anaerobic metabolism. [39]The transition from anaerobic to aerobic metabolism is typical for this phase[39]. Germination is a key process at the beginning of the life of a new individual plant. Therefore, all interventions that affect their course are a decisive factor for the life condition of plants and the quality of the products obtained from them.

In this context, defining a reproducible 'plasma dose' remains a significant challenge for the field. Most studies rely on 'treatment time' as a proxy for dose[12,19,40–43], which fails to account for variations in discharge power and microfilament distribution. To address this, we have recently designed and implemented a new reactor concept that allows plasma-assisted seed treatment under well-controlled conditions[46]. Since seeds can be treated individually (in batches of 1 to 5 seeds), it is possible to precisely determine the plasma dose according to the approach proposed in[46]. In addition to controlling the pressure, composition, and humidity of the working gas, the reactor allows for the precise determination of not only the total power dissipated in the plasma, but also the total energy used to treat a single seed and the time the seed remains in physical contact with the plasma phase (which is usually very different from the commonly reported parameter called exposure time). The plasma phase is then locally characterized, for example, by the distribution of UV A-B-C radiation, the densities/parameters of reactive species, changes in electric fields, or changes in the gas temperature that trigger co-biological responses.

The remainder of this paper is organized as follows. Section 2 describes the experimental setup and the utilized diagnostics. The discussion of the results is in Section 3. It contains electro-optical analysis of the discharge, study of changes in surface chemistry and morphology, and concludes with the effects of these changes on the biological properties of the seeds (germination speed, root length, etc.). The paper is concluded in Section 4. Finally, to ease comparison and reproducibility across plasma treatment experiments, the basic characteristics of the setup, samples, and a list of electrical and plasma parameters characterizing the treatment and post-treatment testing are presented in Supporting Information in Table S1, which serves as the treatment protocol proposed by Waskow[46].

Experimental setup, materials, and methods

Volume DBD reactor and seed treatment

Figure 3a illustrates the compact and modular volume dielectric barrier discharge (DBD) reactor employed in this research. The reactor features two circular alumina dielectrics (Ø = 2.54 cm) mounted on polylactide (PLA) holders, which are securely

View Article Online
DOI: 10.1039/D5FB00081A

sealed within a main reactor body[13,43,45]. Silver-based electrodes (Ø = 2.1 cm) cover the opposing sides of the discs, facilitating discharge generation in the space enclosed by the alumina discs. The adjustable holders, depicted in Figure 3b, enable straightforward sample insertion, easy replacement or cleaning of the dielectrics or electrodes, and, crucially, adjustment of the discharge volume gap. The gap size is determined by a specific spacer (Figure 3b), which is initially placed to ensure the outer collar is correctly positioned. This slip-on collar then limits the insertion depth of the grounded electrode into the chamber, ensuring precise and consistent electrode placement during repeated insertions and seed replacements after treatment. The specific discharge gap of 5 mm results in the direct and focused treatment of samples (Figure 3c).

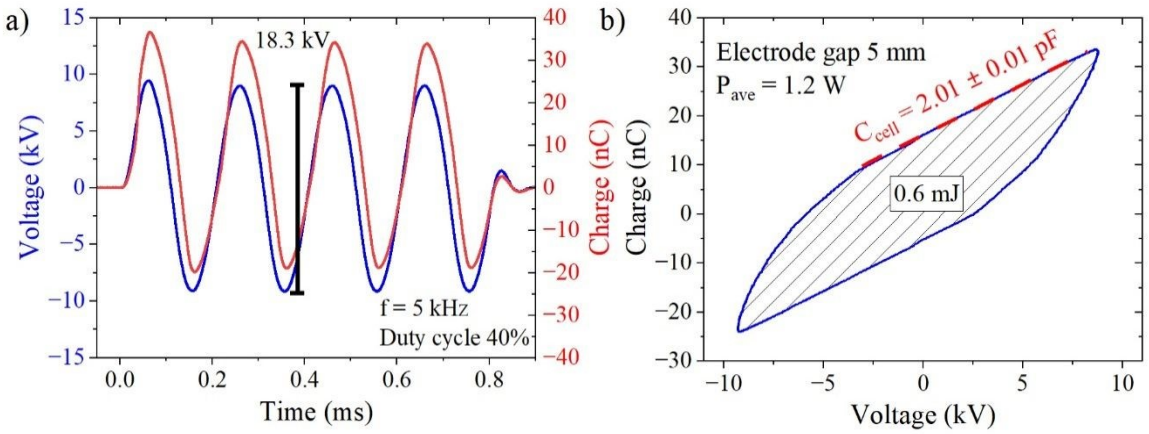

Figure 4: Basic electrical characteristics a) time evolution of applied voltage and transferred charge during one HV burst and (b) corresponding Lissajous figure (Q-V plot) with calculated values of average power (P_{ave}) and reactor capacitance (C_{cell}).

Opto-electrical discharge diagnostics

The reactor was powered using a combination of a TG1010A Function Generator (Aim-TTi, Ltd., Huntingdon, Cambridgeshire, UK), a Powertron Model 1000A RF Amplifier (Industrial Test Equipment Co., Inc., Port Washington, NY, USA), and a high-voltage step-up transformer. A sinusoidal high-voltage (HV) waveform at a frequency of 5 kHz was modulated by a square waveform at 500 Hz, maintaining a fixed duty cycle of 40% to prevent excessive seed heating during exposure. This configuration produced four consecutive HV sine waves (each 0.8 ms), followed by a 1.2 ms cooling period. During all plasma treatments, synthetic air (Scientific, Messer, Bad Soden, Germany; H_2O < 2 ppm, CO + CO_2 < 0.2 ppm) was utilized as the working gas, with a consistent airflow of 1 slm. A Tektronix DPO5204 oscilloscope (Tektronix, Inc., Beaverton, OR, USA) with a bandwidth of 2 GHz and a sampling rate of 5 GS/s was employed to capture discharge characteristics, averaging 512 samples to minimize noise. Voltage and transferred charge were measured using a Tektronix P6015A high-voltage probe (1000:1@1 MΩ, bandwidth 25 MHz) and a 316 nF capacitor connected in series. Optical emissions from the discharge area were sampled through two quartz side windows of the reactor (Figure 3a). An Andor iStar ICCD camera DH740i-18U-03 (Oxford Instruments, Abingdon, UK) was paired with an iHR-320 spectrometer (Jobin-Yvon, Horiba Instruments Inc., Edison, NJ, USA), equipped with 300, 1200, and 3600 G mm−1 dispersion gratings. The concentrations of ozone and NOx, the primary products of the plasma process, were measured using a non-dispersive UV absorption ozone monitor (Advanced Pollution Instrumentation Model 450, Teledyne API, San Diego, CA, USA) and a chemiluminescence NOx analyzer (Model T200H, Teledyne API, San Diego, CA, USA), respectively.

Post-treatment seed surface analysis

The surface chemical composition of plasma-treated seeds was analyzed using X-ray photoelectron spectroscopy (XPS). Measurements were performed with an AXIS Supra spectrometer (Kratos Analytical Ltd., UK) equipped with a monochromatic Al Kα source (1486.6 eV). XPS spectra were acquired from an area of approximately 700 × 300 μm² at a fixed takeoff angle of 90°. Survey and high-resolution spectra were collected with pass energies of 80 eV and 20 eV, respectively. Surface charging was compensated using an electron flood gun. The acquired spectra were processed with CasaXPS software, applying Shirley background subtraction and Gaussian peak fitting with variable widths. Peak positions were determined with a precision of ± 0.2 eV. The C 1s hydrocarbon peak at 284.5 eV was used as the reference for binding energy calibration[47]. For statistical analysis (calculation of mean and standard deviation), each barley seed (4 samples in total) was cut into two pieces and fixed to the XPS sample holder using Cu tape.

The nature of the low-temperature treatment ensures that its impact is largely confined to the seed surface rather than the bulk. To accurately assess the effect of plasma treatment on barley seeds and to focus exclusively on the chemical composition of the surface without contributions from the bulk material, we employed the surface-sensitive technique of X-ray photoelectron spectroscopy (XPS). Two seeds were used for each experimental condition. Surface analysis using XPS was supplemented with energy-dispersive X-ray spectroscopy (EDX) to determine the distribution of measured elements on the seed surface.

Open Access Article. Published on 15 June 2026. Downloaded on 6/15/2026 11:33:03 PM.
This article is licensed under a Creative Commons Attribution 3.0 Unported Licence.

Sustainable Food Technology Accepted Manuscript

This journal is © The Royal Society of Chemistry 20xx

Please do not adjust margins

View Article Online
DOI: 10.1039/D6FB00081A

Open Access Article. Published on 15 June 2026. Downloaded on 6/15/2026 11:33:03 PM.
This article is licensed under a Creative Commons Attribution 3.0 Unported Licence.

To assess the wettability of the barley seed surface, drop shape analysis was performed using the sessile drop method with a custom-made device (consisting of a syringe for the droplet deposition, a sample holder, and a camera connected to a computer). The device was used to capture images of the droplets on untreated and treated seeds. Static contact angles were obtained from images taken immediately after the droplet deposition (using the built-in three-point fitting routine). All contact angle measurements were performed in laboratory air at room temperature. A single droplet (5 µL, water and methylene iodide) was carefully placed onto the smoother (dorsal) side of an individual barley seed surface. The resulting contact angles were calculated as the mean and standard deviation of 10-15 separate values (one for each seed). Surface energy, with its dispersive and polar components for the seed surfaces, was then estimated using the Owens-Wendt-Rabel-Kaelble (OWKR) model[48,49] from the respective contact angles of the utilized liquids (the dispersive and polar components of both liquids' surface energies are in Table S2).

Post-treatment seed 'biotesting'

In this study, we used Spring barley kernels (*Hordeum vulgare L., 'Malz'*, country of origin: Czech Republic, harvest year 2024, untreated, obtained from Limagrain s.r.o.). Prior to the treatment, the seeds were stored in the dark, at room temperature conditions. The type used in this work is a variety of early-maturing spring barley belonging to the group of varieties used for the production of malt suitable for beer production with the Protected Geographical Indication "Czech beer"[50]. For this use, cereals must have a high grain germination capacity (at least 95%), low protein content, high malt extract, uniform grain size, and high activity of the degrading enzymes, beta- and alpha-amylases, for the natural ethanol fermentation process.

Water uptake during the imbibition phase. Sets of 14 kernels for each variant were placed in glass beakers, and 14 mL of deionized water was added to each beaker. The kernels were surface dried, and the weight of the kernel sets was measured every 15 minutes. After measuring, the kernels were returned to the beakers, and 14 mL of deionized water was added again. The experiment was conducted at a temperature of 20 ± 1 °C in light for 10 hours.

Germination tests. Petri dishes (14 cm diameter) were lined with 2 layers of filter paper. The experiment was evaluated in 4 biological replicates, with a minimum total of 48 kernels per variant. All kernels were laid out with the hilar groove down, and then the filter paper was soaked with 20 mL of deionized water. Samples were incubated in the dark at a temperature of 20 ± 1 °C for 3 days. The number of germinated kernels was evaluated every day (the kernel was considered germinated when a root was visible). From the results the means and standard errors of these parameters were calculated according to Šerá[51]: *germination energy* (percent of germination [%]), *germination index* (expressed as the sum of the ratios of the number of germinated kernels and the corresponding number of hours of the experiment duration. Given by the formula $n_1/24 + n_2/48 + n_3/72$ [a.u.]) and *germination rate* (ratio of the percentage of the kernels germinated at the beginning and in the end of the experiment. Given by the formula $n_{24}/n_{72}*100$ [%]). At the end of the experiment, the fresh weight of all kernels (both ungerminated and germinated) was evaluated. Consequently, the samples were dried at 80 °C until a constant weight for dry weight determination.

For comparison, the germination test was also performed according to Czech State Standard number 46 1011-13. The kernels were incubated in a 0.75% H_2O_2 solution (1 ml of solution/grain) under the same laboratory conditions. The peroxide solution was changed after 48 hours, germination was assessed after 72 hours, and expressed as the ratio of germinated kernels to their total number [%].

Dynamics of root system growth. Petri dishes (14 cm diameter) were lined with 2 layers of filter paper. The experiment was evaluated using 10 germinating kernels per variant to calculate the mean and standard error. All kernels were laid out with the hilar groove down, and then the filter paper was soaked with 20 mL of deionized water. Samples were incubated in the dark at 20 ± 1 °C for 3 days. A photo of the Petri dishes with germinating kernels was taken every day. The total length of the roots [cm] per kernel was subsequently measured using image analysis (ImageJ, National Institute of Health, USA).

Results and discussion

Discharge characteristics

The VDBD reactor utilized in this study (Figure 3a), with seeds placed in the interelectrode space, results in the direct treatment of samples (Figure 3c), which exposes the seed to both the luminescence (UV and visible) and highly reactive compounds (mainly RONS and energetic ions) generated by the plasma[52]. The choice of direct treatment by VDBD geometry enables the highest energy transfer between the plasma and the samples[5]. This energy efficiency is further enhanced by the specific selection of electrode gap and applied voltage, which were chosen in accordance with previous research[45] that quantified the particular energy dose delivered to each seed. The peak-to-peak voltage of 18.3 kV was identified as insufficient to generate microdischarges (MDs) in the empty 5 mm electrode gap; however, it permits breakdown in the region of the seeds, as their presence reduces the effective electrode gap and locally intensifies the electric field around the sample surface[53–55]. Under these conditions, MDs, and consequently direct treatment of samples, occur only on the upper and lower surfaces of the seed, as shown in Figure 3 c), and previously demonstrated using 2D imaging[45]. Figure 4. a) shows one HV burst composed of 4 consecutive waves and the corresponding charge transferred through the system (measured by a capacitor connected in series). This burst mode, unlike continuous AC cycles, creates a periodic cooling time without any MDs during the treatment and has been found to be effective for treating heat-sensitive samples, as it ensures stable treatment conditions by maintaining a low gas temperature and operating at low airflow rates, even over extended exposure times (several minutes).

The energy transferred into the system during plasma treatment has been calculated using the Lissajous figure method[56], in which the energy deposited by the plasma equals the area of the QU-plot (charge-voltage). This method is generally more accurate in the estimation of filamentary discharge power in comparison to the simple integration of the voltage-current product, which tends to

Sustainable Food Technology Accepted Manuscript

View Article Online
DOI: 10.1039/D6FB00081A

Open Access Article. Published on 15 June 2026. Downloaded on 6/15/2026 11:33:03 PM.
This article is licensed under a Creative Commons Attribution 3.0 Unported Licence.

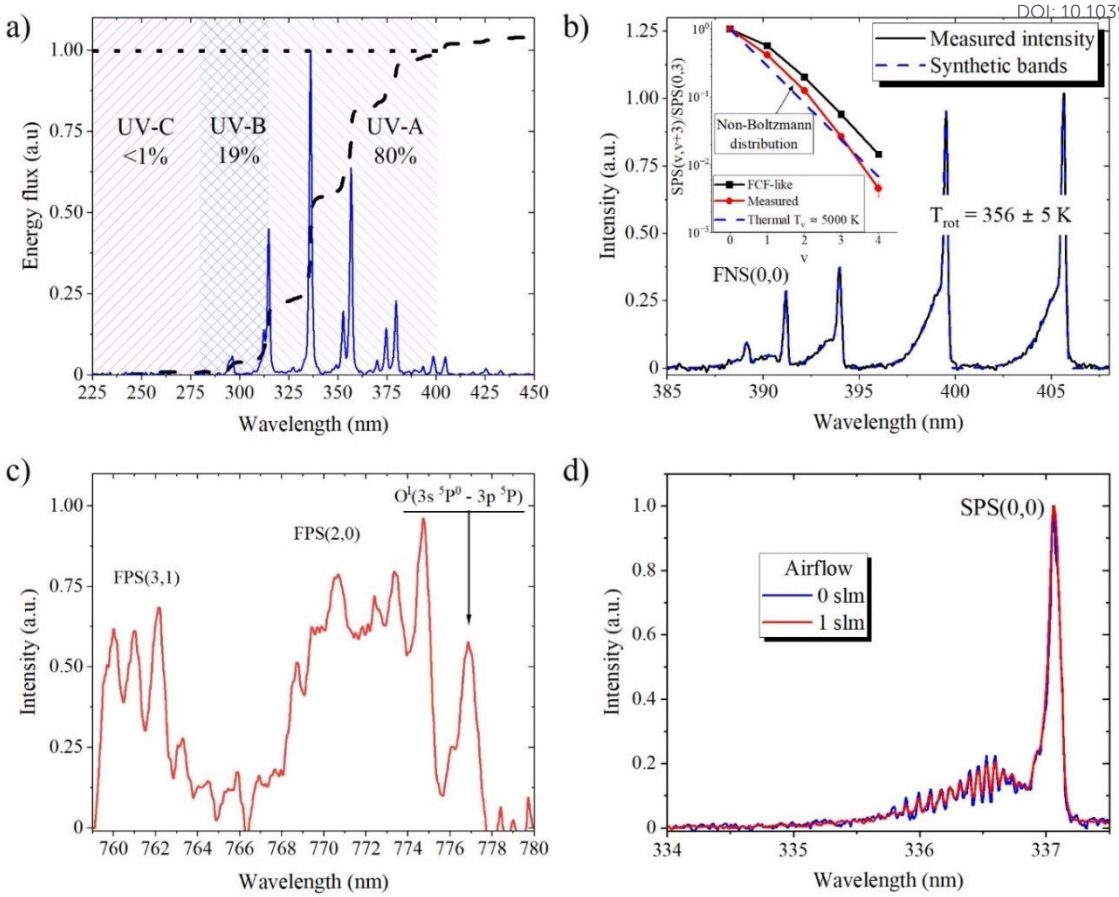

Figure 5: a) The characteristic UV emission spectrum with its three subtype regions (A, B, and C) highlighted. The dashed line represents integrated emission with ratios of individual UV subtypes marked. b) The emission spectra from SPS Δv = -3 sequence and FNS(0,0) averaged over HV-burst compared to the synthetic bands with T_{rot} = 356 ± 5 K. The inset figure displays the determined vibrational distribution function of $N_2(C)$ compared with FCF-like and thermal distributions (T_{vib} = 5000 K). c) the vis-NIR region of the first positive system of N_2 (FPS), vibronic bands (2,0) and (3,1) with a clear O^I line at 777 nm. d) The effect of airflow on the $N_2(C, v = 0)$ state.

underestimate the average DBD power due to the insufficient current probe bandwidth[57]. The graphical representation of the Lissajous figure integration is shown in Figure 4 b). The average discharge power was determined to be 1.2 W (energy of a single HV sine wave is 0.6 mJ, frequency 5 kHz, and duty cycle 0.4). The slope of the plot in Figure 4 b) (red dashed line), which corresponds to the capacitance of the reactor in the absence of the discharge[58] (≈2 pF), is in agreement with the previous studies[45] performed with this geometry and seed filling (3 seeds, 5 mm gap), indicating the reproducibility of the treatment conditions from an electrical standpoint. The localization of the MDs around the individual seeds can be used to more accurately assess the average energy dose delivered by plasma. Given the number of seeds and range of treatment times from 5 to 300 s, we can estimate an average plasma dose per seed to be between 2 and 120 J/seed. Furthermore, if we simplify the seed shape to a prolate spheroid, we can estimate the average surface area[59] to be around 60-80 mm^2[59], giving us an estimate of the total surface energy dose range 0.025-1.5 J/mm^2 from the shortest to the longest treatment time. All energy dose calculations, however, serve only as an upper estimate, as not all energy spent by plasma is meaningfully utilized for the treatment of samples.

Optical emission spectra from the UV to vis-NIR wavelength region were collected from the area around the top half of the middle seed (located closest to the vertical axis of the DBD reactor) and focused using a series of lenses and iris diaphragms. Two regions hold particular interest in terms of plasma treatment: the UV-to-blue region (200-500 nm) and the red-to-NIR region (750-900 nm). The former region contains emission bands of molecular nitrogen N_2 and N_2^+, which are critical for determining fundamental plasma parameters such as gas temperature and reduced electric field[60], while the latter region contains atomic lines of nitrogen and oxygen[61], serving as indicators of dissociation levels in plasma filaments, which are important for the formation of plasma products (mainly reactive oxygen and nitrogen species). Figure 5 shows all the time-averaged emission spectra acquired in the indicated region of interest. Figure 5a covers the entire UV region (200-400 nm) detectable under atmospheric-pressure conditions, before atmospheric oxygen absorption starts to play a role. The intensities of detected emission, mainly consisting of second positive and first

Sustainable Food Technology Accepted Manuscript

This journal is © The Royal Society of Chemistry 20xx

Please do not adjust margins

View Article Online
DOI: 10.1039/D5FB00081A

Open Access Article. Published on 15 June 2026. Downloaded on 6/15/2026 11:33:03 PM.
This article is licensed under a Creative Commons Attribution 3.0 Unported Licence.

negative systems of nitrogen, were integrated along the 200-400 nm interval (dashed line in Figure 5a and normalized to determine the ratios of UV-A (320-400 nm), UV-B (290-320 nm), and UV-C (200-290 nm) components of the total UV energy flux, which are often mentioned as contributing factors, both positive and negative, in plasma treatment. UV-C is noted for its germicidal properties[62], while UV-B is strongly absorbed by DNA and can potentially induce DNA lesions[63].

Although self-repair mechanisms in plants tend to mitigate serious damage. From Figure 5a**,** we can see that the majority of UV energy flux is taken by UV-A, while UV-B takes approximately 20%, and UV-C contribution is energy-wise minimal (due to the absence of NO-γ($A^2\Sigma^+ \rightarrow X^2\Pi_r$) emission). Figure 5b contains slightly higher resolution spectra of a specific UV interval (385-410 nm), which contains bands of a single SPS sequence (Δv= -3) and FNS(0,0) band. By fitting this spectrum with a synthetic model spectrum, we can determine the rotational temperature (T_{rot}) and vibrational distribution function (VDF) of $N_2(C)$ state. The obtained shape of VDF (inset figure in Figure 5b doesn't follow the thermal distribution (blue dashed line), and thus, the vibrational temperature of the $N_2(C^3\Pi_u)$ state cannot be defined. However, the higher vibrational levels roughly correspond to the populations expected for pure electron-impact excitation from the ground electronic state (Frank-Condon factor-like or FCF-like distribution), suggesting weak contributions from other mechanisms

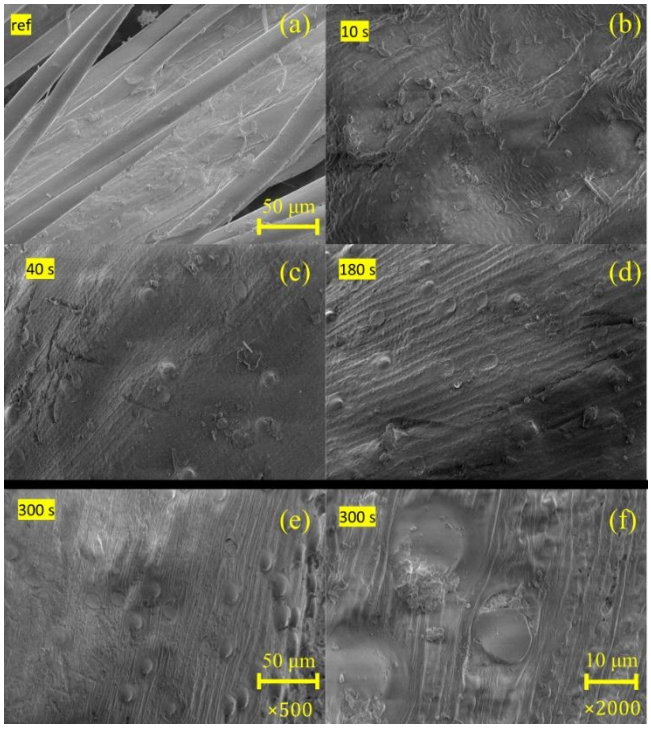

Figure 6: SEM images (500x magnification) indicating the change in surface morphology due to plasma treatment. (a) reference surface, (b-e) after 10s, 40, 180, and 300 s of plasma treatment, (f) 300s treatment with increased magnification (2000x).

to the population of the $N_2(C)$ state and therefore allowing us to use the determined T_{rot} = (356 ± 5) K as an estimate of the background gas temperature. Figure 5c) displays the part of the vis-NIR region containing the bands of the first positive system (FPS) of nitrogen and a clearly distinguishable triplet of atomic oxygen at 777 nm. Atomic oxygen is arguably the most significant contributor to changes in the elemental structure and, subsequently, the properties of the treated seed surface (further analysis is presented in the section dedicated to Surface morphology and chemistry). However, as the dissociation level in the MDs is quite low, along with temperature, the oxygen triplet remained the only observable atomic line emission in the spectra. Figure 5d illustrates the effect (or lack thereof) of airflow on the shape of the SPS(0,0) band and thus the rotational temperature. The band shape changes only slightly between the static gas condition (0 slm airflow) and the standard 1 slm used across all other experiments. The flow of gas, therefore, mainly prevents the accumulation of plasma products (RONS) and replenishes the reactor chamber with fresh air, while its contribution to system cooling is minimal.

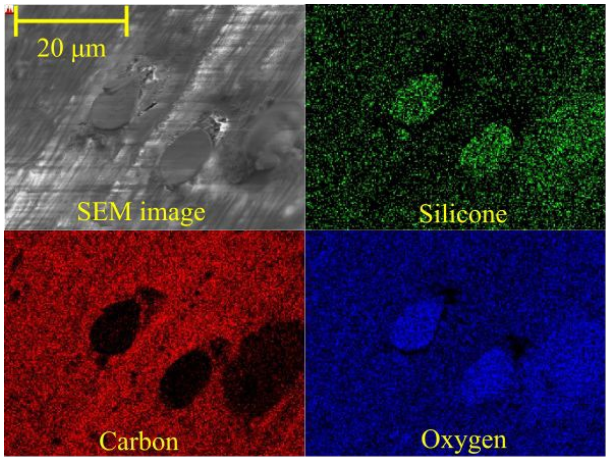

Figure 7: Images of barley surface treated in plasma for 300 s: SEM image, and EDX images with distribution of carbon, silicon, and oxygen.

Surface morphology and chemistry

The surface morphology of barley seeds was investigated using SEM both prior to and following DBD plasma treatment. Figure 6 presents SEM images at 500× magnification, illustrating the seed surfaces before and after plasma exposure for 10 s, 40 s, 180 s, and 300 s, respectively. A detailed examination of the microstructure on the reference sample (Figure 6a) reveals a surface with some visible hairs, with no discernible changes noted after a 10-second plasma treatment (Figure 6b). A 40-second plasma exposure resulted in the slight emergence of circle-shaped dots, bumps, or craters, each approximately 15 microns in diameter (Figure 6c). Extending the plasma treatment to 180 seconds revealed a greater abundance of these features (Figure 6d), whereas a 300-second treatment led to a significant increase in the number of dots and bumps (Figure 6e). Figure 6f showcases the surface of a seed treated with 300 seconds of plasma at a higher magnification of 2000x, providing a clearer view

Sustainable Food Technology Accepted Manuscript

View Article Online
DOI: 10.1039/D5FB00284A

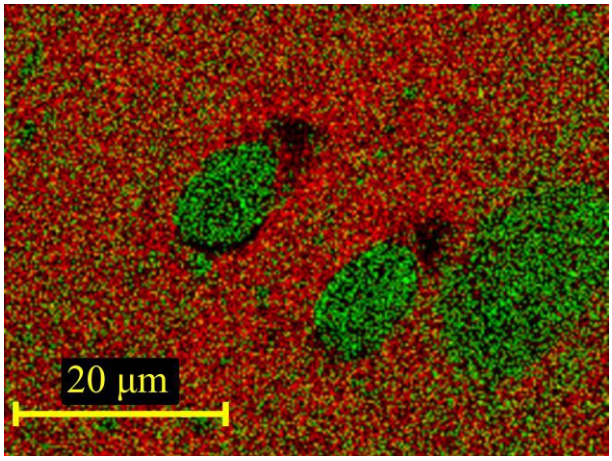

Figure 8: Image of barley seed treated in plasma for 300 s showing both the distribution of carbon (red) and silicon (green).

of these morphological changes. The observed features are likely localized ablation sites caused by the directed impingement of plasma microfilaments onto the seed coat. As treatment time progressed to 180 s and 300 s (Figure 6d-e), the density of these etching craters increased significantly. This proliferation indicates cumulative surface modification, leading to a substantial increase in micro-roughness.

EDX was specifically utilized to ascertain the chemical nature of the dot/bump structures that emerged after 180 s and 300 s of plasma treatment. Figure 7 provides a visual representation of the elemental distribution on the surface of barley seeds that underwent a 300-second treatment. The EDX image of a barley seed subjected to 300 seconds of plasma reveals the distribution of carbon (depicted in red) and silicon (depicted in green). It appears that the plasma treatment led to a non-homogeneous etching process, creating areas with higher silicon concentrations and notably lower carbon concentrations. These areas may indicate potential voids or holes in the seed's surface, thereby exposing the bulk of the seed, which has a higher silicon content (Figure 8).

The presence of silicon in seeds, specifically in barley seeds, is not an unexpected discovery, as has been previously documented by other researchers. For example, Ma et al.[64] conducted a study investigating genotypic variation in silicon concentration in barley grain, underscoring the relevance of silicon to seed composition. Azizi et al. [65], when analysing the composition of wheat husks, found that up to 85% of the ash mass is made up of silicon dioxide. Oxides of potassium, calcium, iron, and magnesium are also present to a greater extent. Silicon in insoluble forms is stored mainly in the cell walls on the inner side of the epidermis and functions as a barrier against the entry of various (mainly fungal) pathogens and insect pests[66]. Silicon is also involved in the formation of bonds between lignin and carbohydrates via the associations with phenolic acids or aromatic rings in cell walls. In addition, silicon is stored in the cell walls in phenol-carbohydrate complexes or in the form of silicone gel[67,68]. The positive effects of exogenously applied silicon on embryo viability, germination-related processes, and subsequent plant development, especially under stress conditions, are well known[69–71]. Exogenously applied silicon helps mitigate the negative impacts of abiotic stresses (drought, environmental toxicity, etc.) and enhances nutrient mobilization in seeds by increasing the activity of hydrolytic enzymes. Its positive effect on germination has also been studied in connection with the modulation of phytohormone levels (GA, ABA, JA)[72].

To accurately assess the effect of plasma treatment on barley seeds and to focus exclusively on the surface chemical composition, unaffected by contributions from the bulk material, we employed the surface-sensitive technique of XPS. The low-temperature nature of the treatment ensures that its impact is largely confined to the seed surface rather than the bulk. Figure 9 presents the atomic concentrations (in at.%) of the main surface elements and their evolution during plasma treatment. Table S3 shows the XPS data used for Figure 9. The dominant surface elements in untreated barley seeds are carbon (88.8 ± 1.7 at.%) and oxygen (9.2 ± 1.4 at.%), with minor amounts of nitrogen, silicon, calcium, and potassium. After 10 s of plasma treatment, oxygen increases to 21.8 ± 2.0 at.%, while carbon decreases to 74.4 ± 3.2 at.%. Minor increases are also observed in nitrogen, silicon, calcium, and potassium. At 40 s, oxygen continues to rise to 35.1 ± 0.6 at.%, with carbon dropping to 53.5 ± 0.5 at.%. A notable increase in silicon (7.0 ± 2.8 at.%) is observed, and traces of sodium become detectable only after 10 and 40 s of treatment. After 180 s, oxygen becomes the dominant element (52.4 ± 3.8 at.%), while carbon decreases markedly to 25.5 ± 7.6 at.%. Silicon further increases to 14.7 ± 4.4 at.%, accompanied by small rises in nitrogen, calcium, and potassium. Following the longest exposure (300 s), oxygen reaches its maximum level (57.9 ± 1.9 at.%), carbon declines to its lowest value (16.6 ± 1.8 at.%), and silicon increases to 18.7 ± 3.3 at.%. Other elements also show further increases, and, uniquely at this stage, traces of magnesium and phosphorus are detected. Elements such as iron, calcium, magnesium, and potassium are essential nutrients for plant growth and stress tolerance[73], and their imbalance in seed volume could negatively affect the final germination rate. However, the XPS mostly detects the surface chemistry of the dead outer layer, whose elements are not utilized for germination.

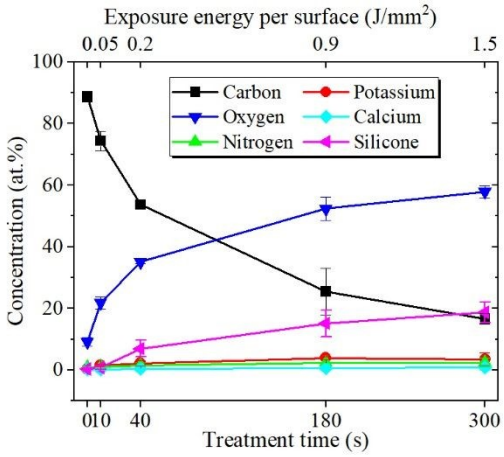

Figure 9: The effect of plasma treatment time (0-300 s) on the chemical surface composition of barley seeds.

Open Access Article. Published on 15 June 2026. Downloaded on 6/15/2026 11:33:03 PM.
This article is licensed under a Creative Commons Attribution 3.0 Unported Licence.

Sustainable Food Technology Accepted Manuscript

This journal is © The Royal Society of Chemistry 20xx

Please do not adjust margins

View Article Online
DOI: 10.1039/D5FB00081A

Open Access Article. Published on 15 June 2026. Downloaded on 6/15/2026 11:33:03 PM.
This article is licensed under a Creative Commons Attribution 3.0 Unported Licence.

Sustainable Food Technology Accepted Manuscript

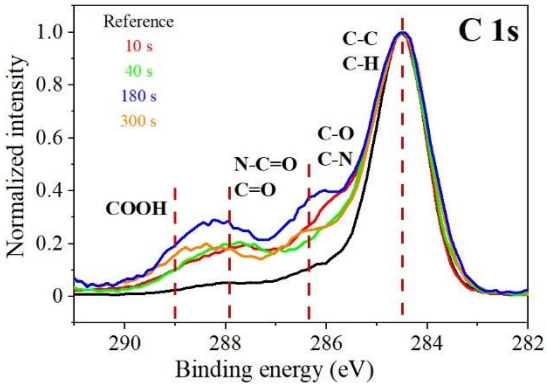

Figure 10: The effect of plasma treatment (0-300 s) on C 1s high-resolution XPS peaks of barley seeds.

Rapid depletion of surface carbon, accompanied by pronounced oxygen enrichment, represents a robust and recurrent signature of atmospheric plasma treatment across a wide range of seeds, including quinoa, barley, pea, and oil-seed rape[13,47,74,75]. XPS studies consistently attribute this behavior to oxidative etching and chemical transformation of lipid- and polysaccharide-rich outer seed coat layers, driven by plasma-generated reactive oxygen and nitrogen species, rather than to thermal degradation or bulk modification. In parallel, several works employing XPS depth profiling and gas cluster ion beam (GCIB) sputtering have demonstrated a progressive enrichment of mineral elements such as K, Ca, and Si in the near-surface region, providing direct evidence for plasma-induced ion migration toward the negatively charged seed surface formed within the plasma sheath, rather than surface contamination or simple exposure of the bulk composition[76]. Importantly, the evolution of surface composition with treatment time is frequently non-linear: at extended plasma exposures, partial saturation, redistribution, or even attenuation of some elemental changes has been observed in barley, pepper, melon, and *Brassica* sp. seeds[47,74]. This behavior has been interpreted as a transition from initial surface functionalization and selective carbon removal to partial over-etching and structural reorganization of the seed coat. From a mechanistic standpoint, these observations are fully consistent with the current physical model of plasma–seed interaction, in which plasma sheath formation induces negative surface charging, promotes electromigration of mobile cations, and enables preferential removal of weakly bound organic carbon while leaving the seed bulk largely unaffected.

The high-resolution XPS peaks of C 1s, O 1s, N 1s, Ca 2p, and Si 2p (see Figure 10 and Figure S1 a-d in Supporting Information) were analyzed for Barley seeds before and after plasma treatment. The comparison of the C 1s peaks (Figure 10) revealed a significant difference between untreated and plasma-treated seeds, characterized by visible changes in the shape of the carbon peaks at the higher binding energy (BE) region. The increase in intensity in the higher BE region in the shoulder indicates notable chemical changes induced by plasma treatment. For a better understanding of the changes in the C 1s peaks, the normalized C 1s peaks were analyzed with respect to the contribution of different carbon bonds. The main component in the C 1s peaks is attributed to C-C/C-H bonds located at 284.5 eV. The component for C-O/C-N bonds is observed at 286.3 eV, for N-C=O/C=O bonds at 287.9 eV, and for COOH bonds at 289.0 eV[13]. Comparing the intensities of carbon-containing components in untreated and plasma-treated seeds enabled estimation of the plasma treatment's influence on the seed surface.

High-resolution XPS C 1s spectra of barley seed surfaces subjected to atmospheric-pressure air plasma for 10, 40, 180, and 300 s demonstrate a pronounced, non-linear restructuring of surface carbon chemistry (Figure 9). The untreated reference surface is dominated by the hydrocarbon component at ≈284.8 eV, corresponding to C-C/C-H bonds characteristic of lipid- and wax-rich layers forming the outer pericarp. This is consistent with previous

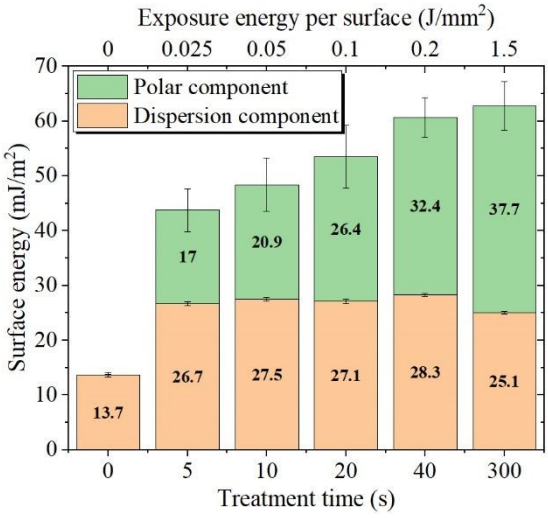

Figure 11: The effect of plasma treatment time on the polar and dispersion component of the seeds' surface energy calculated by the OWRK method from the average contact angles of the DI water and diiodomethane on 10-15 seeds.

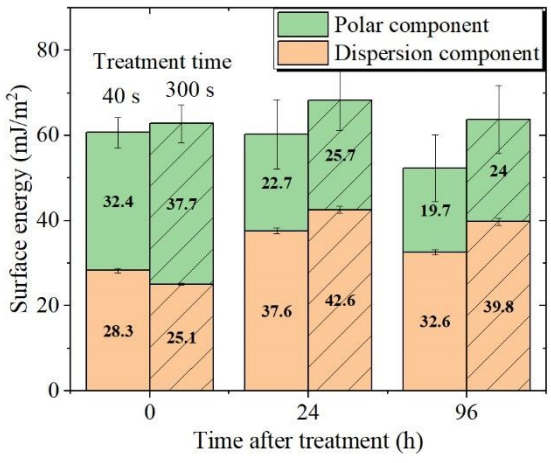

Figure 12: The effect of aging (24 and 96 h after treatment) on the components of the seeds' surface energy. The patterned bar corresponds to 300 s of plasma treatment, while the bar without a pattern corresponds to 40 s.

Please do not adjust margins

View Article Online
DOI: 10.1039/D5FB00084A

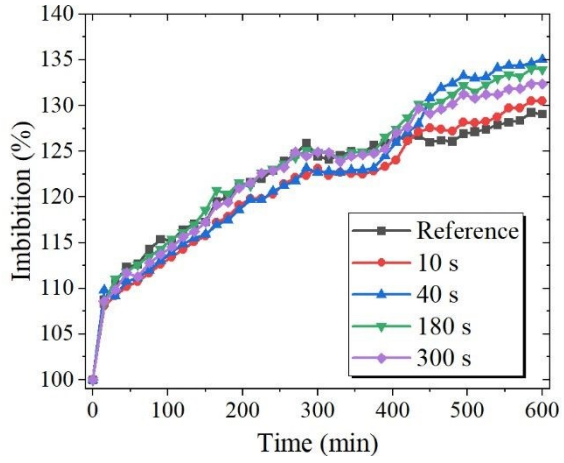

Figure 13: The effect of plasma treatment on the imbibition of barley seeds in the first 10 hours in DI water (1 ml/seed) under laboratory conditions.

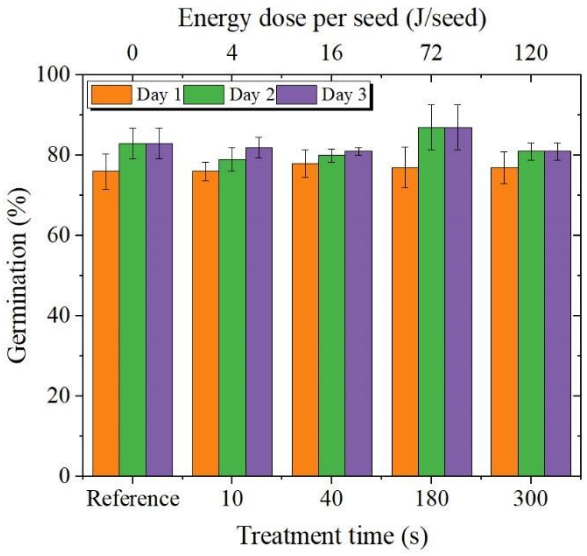

Figure 14: The germination of plasma-treated barley seeds compared with the untreated reference sample under laboratory conditions.

XPS analyses of pea seed coats, which report a predominantly aliphatic carbon signature prior to plasma exposure[75].

Upon plasma treatment, a decrease of the C-C/C-H contribution is observed, accompanied by the emergence and growth of higher-binding-energy components associated with oxygen- and nitrogen-containing functional groups. The component centered at ~286.0 eV is assigned to C-O and C-N bonds, indicating the incorporation of hydroxyl, ether, and amine functionalities. Further oxidation is evidenced by the development of features at ~287.6–288.0 eV, attributable to carbonyl (C=O) and amide-type (N-C=O) species, while the high-energy tail near ≈289.0 eV reflects the formation of carboxylic (COOH) groups. Such chemical evolution is a characteristic of air-plasma interaction with organic biopolymers and arises from reactions driven by reactive oxygen and nitrogen species (RONS), including atomic O, O_3, ·OH, NO_x, and plasma-generated UV radiation[10,43]. The previous experiments with the setup[13,43,45] showed minimal production of NO_x (3-30 ppm, depending on the gap distance, while O_3 concentration in outlet gas reached as high as 600 ppm. Thus, among the long-lasting RONS, ozone has the principal effect on surface-chemistry modification.

Importantly, the C 1s spectral evolution correlates with elemental composition results, showing a significant decrease in total surface carbon content, which confirms that plasma treatment not only functionalizes the surface but also induces partial ablation and volatilization of carbon-rich material. The removal of low-binding-energy hydrocarbon species via oxidative etching and desorption of CO and CO_2 has been widely reported for plasma-treated seeds and biopolymeric surfaces, particularly under ozone-rich DBD conditions[57,74], as is also the case with the current setup. The time dependence of these modifications is distinctly non-monotonic. Short exposures (10–40 s) already induce measurable oxidation, indicating rapid activation of the outermost organic layer. The most pronounced transformation occurs at 180 s, where oxidized carbon species (C-O/C-N, C=O/N-C=O, and COOH) reach their maximum relative intensities and the C-C/C-H component is most strongly suppressed.

This regime reflects an optimal balance between surface oxidation and retention of a chemically functionalized, yet structurally intact, seed coat. Extending the plasma exposure to 300 s does not further enhance surface oxidation. Instead, a partial reduction in the relative intensity of oxidized carbon functionalities is observed compared to the 180 s treatment. This behavior is consistent with the onset of competing processes at higher plasma doses, including intensified etching of already oxidized moieties, fragmentation of polar functional groups, and progressive removal of the modified surface layer. Similar saturation or reversal effects have been reported for barley, Brassica, Arabidopsis, and quinoa seeds exposed to prolonged DBD plasma treatments, where excessive treatment leads to net loss of functional groups despite increased energy input[13,74,75].

From a mechanistic standpoint, the observed C 1s spectra evolution reflects the interplay of chemical oxidation and physical plasma–surface interactions. Plasma-induced surface charging and sheath formation promote bond scission and oxidation of aliphatic carbon, while simultaneously driving ion migration and redistribution within the near-surface region. Recent depth-resolved XPS studies on barley seeds have shown that such plasma exposure modifies not only O/C and N/C ratios but also induces migration of inorganic cations (K^+, Ca^{2+}) toward the surface, further supporting the interpretation that the plasma affects the seed coat as a coupled organic–inorganic system rather than a purely organic film[76].

Overall, the C 1s spectra unequivocally demonstrate that atmospheric plasma treatment converts the initially hydrophobic, hydrocarbon-dominated barley seed surface into a polar, chemically heterogeneous interface enriched in oxygen- and nitrogen-containing functionalities while simultaneously reducing the total surface carbon content. The maximum functionalization observed at 180 s is therefore highly relevant for downstream biological effects, such as enhanced wettability, faster imbibition, and accelerated early germination, whereas the diminished modification at 300 s highlights the critical importance of plasma dose optimization to avoid over-etching and loss of beneficial surface chemistry.

Open Access Article. Published on 15 June 2026. Downloaded on 6/15/2026 11:33:03 PM.
This article is licensed under a Creative Commons Attribution 3.0 Unported Licence.

Sustainable Food Technology Accepted Manuscript

This journal is © The Royal Society of Chemistry 20xx

Please do not adjust margins

View Article Online
DOI: 10.1039/D6FB00081A

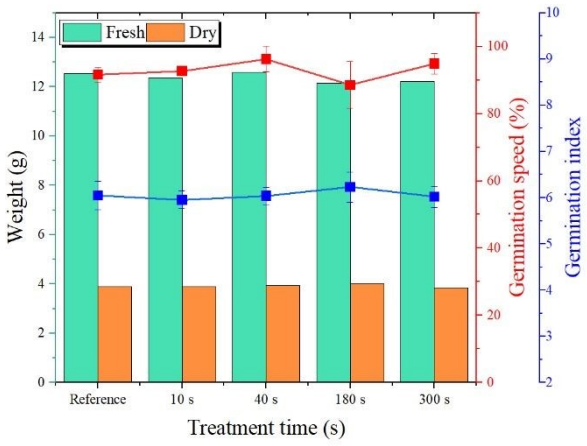

Figure 15: Weight of fresh and dry sample matter after three days of germination (see Figure 14), along with germination speed and germination index of plasma-treated seeds.

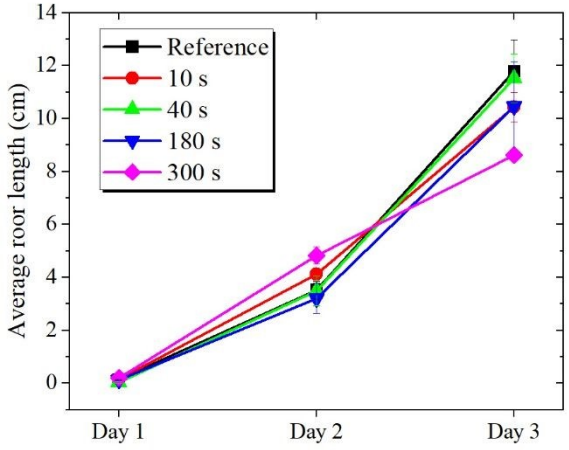

Figure 16: Average root system length of germinated seeds after 1,2, and 3 days.

The comparison and analysis of the O 1s peaks (Figure S1c) revealed significant changes in the shape and position of the oxygen peak for plasma-treated seeds compared to the reference. Notably, the reference O 1s peak has three main components, which may correspond to $CaCO_3$/CaO bonds (~531.2 eV)[77], C-O bonds including Ca-O and Si-O bonds (532.0 eV), and C=O/N-O bonds (533.2 eV)[13]. However, the application of plasma treatment to barley seeds caused a dramatic decrease in $CaCO_3$/CaO bonds and an increase in the other two oxygen-containing components. Moreover, the plasma treatment shifted the O 1s peaks to higher BEs by up to 0.4 eV. This may be due to uncontrolled surface charge or to the redistribution of oxygen-containing bonds. As for the N 1s peaks, the positions of the nitrogen peaks across all samples are rather similar.

The component ascribed to N-H/N-C bonds is located at about 399.5 eV[13] (Figure S1b). The additional component at 402.9 eV is attributed to K-N/Si-N bonds[78] was observed only in long-term-treated barley seed (180 and 300 s). Moreover, in seeds treated for 40, 180, and 300 s, an intense component at 407 eV was observed. This component corresponds to NO_x species[13,47] formed in the plasma through a combination of excited oxygen and nitrogen species. Figure S1a shows the Ca $2p_{3/2}$ and Ca $2p_{1/2}$ peaks detected on the surfaces of both reference and plasma-treated seeds (with a splitting of ≈3.5 eV). The position of Ca $2p_{3/2}$ peaks is located at 346.9 eV, which is attributed to $CaCO_3$/CaO bonds[77] in all samples. Despite the low intensity of the obtained Ca 2p peaks, we may assume that no significant shifts or changes in the shape of the normalized Ca 2p peaks occurred after plasma treatment. Finally, the comparison of obtained Si 2p peaks (Figure S1d) indicates that the position and shape of silicon peaks for untreated and plasma-treated barley seeds remained almost unchanged. According to[79], the position of Si 2p peaks at around 103.0 eV corresponds to SiO_2 bonds.

The change in the water contact angle (WCA) of the seed surface due to plasma treatment is well known[54,80,81]. The WCA tends to drop rapidly from a hydrophobic angle (>90°) to a hydrophilic angle after just a few seconds of treatment as a consequence of a change in elemental composition (as discussed previously) and surface free energy (SFE) of its surface. By measuring the contact angle of at least two liquids (in our case, DI water and methylene iodide), we can calculate the polar and dispersion components of surface energy.

Figure 11 shows the effect of plasma treatment time on both surface energy components. The untreated seeds' surface contains only a dispersion component with polar groups almost completely absent, which supports its hydrophobic properties. Plasma treatment, however, leads to a sharp increase in SFE, which triples and quadruples in comparison to the reference SFE after 5 s and 300 s of treatment, respectively. Also, while the dispersion component remains constant after the initial increase due to 5 s of treatment, the polar component quickly emerges, forming a third of the total SFE after just 5 s and then monotonically (but non-linearly) rises to nearly 60 % of the total SFE after 300 s. The sudden emergence of the polar component of SFE has previously been reported in plasma treatment of pea seeds[80] soybean seeds[82], or rice[54] and is, in general, associated with an increase in O-content on the seed surface, specifically, the formation of C=O, C-O, and COO(H) groups from C-C/C-H bonds as observed by XPS. A strong correlation (r≈0.9) can even be drawn between O-content in Figure 9 and polar SFE in Figure 11. Furthermore, in the SFE calculation, no correction has been made for the unevenness and roughness of the seed's surface (the smoother, dorsal side of the seed has been used to at least partially mitigate it). Nevertheless, the effect of physical morphology cannot be entirely dismissed, as the localized etching of surface microgrooves (as observed by SEM) can further increase wettability by inducing Wenzel-like state[83] onto the already discussed chemical changes.

Figure 12 shows the effect of short aging (1 and 3 days) on SFE to determine the severity of hydrophobic recovery[84] due to reorientation of surface functional groups, reversion of chemical structure, and other mechanisms. The polar component of SFE for both starting treatment conditions (40 s and 300 s) after 3 days reverts to a state comparable to that at 10-20 s of treatment, indicating that their hydrophilic properties are retained over the course of days. Rice seeds treated by VDBD were able to retain their germination rate after 3 days of accelerated aging[85]. Long-term studies on Bambara, chili, and papaya[86] even showed retention of hydrophilicity and increased water uptake after 60 days. It is thus not necessary to plant treated seed immediately after treatment; they

Open Access Article. Published on 15 June 2026. Downloaded on 6/15/2026 11:33:03 PM.
This article is licensed under a Creative Commons Attribution 3.0 Unported Licence.

Sustainable Food Technology Accepted Manuscript

Please do not adjust margins

View Article Online
DOI: 10.1039/D5FB00084A

Open Access Article. Published on 15 June 2026. Downloaded on 6/15/2026 11:33:03 PM.
This article is licensed under a Creative Commons Attribution 3.0 Unported Licence.

Sustainable Food Technology Accepted Manuscript

can be stored and/or transported over several days without significant loss of surface hydrophilicity or water uptake speed.

Seed germination and growth analysis

The key stage of germination is seed imbibition, which is the physical process of water uptake and binding to hydrophilic compounds. In normal (plasma-untreated) barley kernels, imbibition is affected by the hydrophobic character of the husk, which is fused with the *testa* by the lipid-rich cement layer. It is known that the surface and structure of cell walls can be effectively disrupted with (cold) plasma treatment. This not only disrupts the integrity of cell walls but also increases their hydrophilicity[87,88]. Mehta et al. [89] found that cold plasma applied to corn bran caused the disruption of chemical bonds in cellulose, as well as chemical bonds between lignin and carbohydrates, and also chemical disruption of lignin itself. And because the hydrophobic lignin is the main component of barley hulls, the chemical modification of it can significantly affect water uptake by the plasma-treated seed. Figure 13 shows the process of water uptake by the seed (kernel imbibition) over a period of 10 hours. A significant positive effect on water uptake by grains treated with plasma for 40 s, 180 s, and 300 s is observed, but without significant differences between these variants. However, it is interesting to capture the course of imbibing over the measurement time. During the first 7 hours of measurement, the imbibition intensity of the 180 s and 300 s treated variants was comparable to the control sample. On the contrary, treatment with the shortest times led to a lower willingness of the samples to absorb water. Then, a significantly higher dynamics of water absorption were observed in kernels treated with plasma for 40 s - 300 s. At the end of the measurement, these seeds contained almost 10% more water than the reference untreated sample. The increased water absorption of cold plasma-treated soybean seed was also reported by Tomeková et al.[81]. Gruwel et al.[90] studied water uptake and distribution in barley grains using magnetic resonance. They found that at the beginning of imbibition, there is predominantly diffuse water uptake, which increases over a period of approximately 7 hours. Then it slowly decreased, while the amount of water in the kernel remained constant, and its mobility increased, allowing it to distribute to various parts of the kernel. Our results clearly show that the modification of the surface hydrophilicity and integrity of plasma-treated seeds (as described in chapter Surface morphology and chemistry) has a significant effect on the distribution of water in their other parts. Tissue hydration is an integral condition of the germination process associated with the regulation of translation of specific genes and the activation of hydrolytic enzymes. However, excessive and uncontrolled water intake can lead to damage to the seeds, respectively, to the embryos embedded in them[91].

Plasma treatment of barley kernels can affect the germination process not only by modulating hull integrity and hydrophobicity, but also by directly producing ROS and RNS. Natural intensive production of ROS (especially H_2O_2) in dry seeds is a signal for the end of dormancy[92,93]. During the germination process, respectively, after the imbibition, the level of superoxide anion (O_2^-) also increases[38]. Therefore, it could be assumed that ROS generated during plasma discharge (as stated in chapter The optical emission spectra) can also accelerate the germination of treated seeds. However, our results in Figure 15 show that, despite higher water absorption during imbibition (Figure 13), no noticeable effect of plasma on the germination of treated dry barley seeds was observed (see Table S4 in Supporting Information). The reason may be that the ROS in dry seeds are only capable of low mobility, and therefore, they are effective primarily at the site of origin[94]. Thus, the ROS produced via the plasma discharge probably react mainly with the surface layers of the seed, which can form the integrity of the surface of the treated plant material, while simultaneously degrading hydrophobic compounds, such as cuticular waxes. This is also reflected in the reduction of the water contact angle, as confirmed by our results above and the results of many other authors[21,45,80–82,86]. Reducing the impermeability of the surface layers of the plasma-treated seeds also reduces the natural formation of RNS under conditions of anaerobic metabolism[95]. A certain level of NO appears to be essential for the germination process[96], and in non-dormant barley kernels, it continuously increases during imbibition and early stages of germination[38]. Increased ROS production can therefore disrupt the germination process not only by disrupting the seed coat and accelerating the change from anaerobic to aerobic seed metabolism, but also by directly sequestering RNS, thereby reducing their natural levels. On the other hand, during plasma discharge, not only ROS but also RNS are generated. This could explain why no significant effect of different times of plasma treatments on germination parameters was observed in our experiment with dry non-dormant barley kernels (Figure 15). A slight positive effect of plasma discharge treatment on the total number of germinated seeds was observed only in the variant treated for 180 s. However, no statistical significance compared to the other variants, including the control, was found (Figure 14). This is in partial agreement with previously published results by other authors, who state that the effect of direct DBD plasma shows enhanced germination rates, especially in the first 24 h, but after 72 h, no significant difference can be observed[47]. More significant differences between the individual variants were observed in root system length (Figure 16). This was observed mainly on the third day of measurement (Figure S2), when the variant treated for 300 s showed approximately 1/3 lower root length compared to the other variants. A less significant reduction in the root system was also evident in the variant treated by plasma discharge for 180 s. This damage to the root system could be consistent with more severe damage to the seed coat layers of these variants (especially 300 s) and, at the same time, with higher ROS production. As mentioned above, supraoptimal levels of ROS cause oxidative stress in plants, including seeds. For example, in sunflowers, excessive concentrations of ROS in embryonic cells can lead to the development of abnormal seedlings[94]. Moreover, in our experiment, a higher silicon content was also recorded in the 300 s variant. And it is known that the negative effects of ROS in plants can be reduced by increased silicon intake[97]. Also, exogenous application of silicon nanoparticles can increase germination and seedling viability. The possible formation of various nanoparticles is also associated with the effect of plasma discharge[98]. From the overall results presented, it can be concluded that the individual negative and positive effects of plasma treatment on barley seeds can cancel each other out.

However, it is also necessary to note that the effects of plasma treatment on seed germination and seedling development depend

This journal is © The Royal Society of Chemistry 20xx

Please do not adjust margins

View Article Online
DOI: 10.1039/D6FB00081A

on many external and internal factors. These include external conditions of the experiment, such as air humidity or discharge duration, as well as internal conditions, such as seed age or developmental stage. This is proven, for example, by experiments by Attri et al.[99] who found that plasma-generated ROS and RNS can accelerate germination of older radish seeds (maximum germination percentage) and stimulate seedling growth, and our not-yet-published results from experiments with dormant and non-dormant barley kernels treated with plasma discharge in different humidity conditions. The influence of humidity on the plasma treatment effect on seed germination and seed dormancy breaking has been studied, for example, in lettuce seeds[100]. It was found that humidity plays an important role in ROS production. The modulation of 'biological age' of the seeds (dormancy or plasma-induced senescence) is also crucial for the content of substances that are naturally able to scavenge superoxide anions. Another parameter that has a significant impact on the final effect of plasma treatment is the discharge duration. As already mentioned, it affects the content of ROS and RNS and, directly or indirectly, the expression of genes involved in plant antioxidant mechanisms[101].

Conclusions

In this work, we studied the effects of direct plasma treatment using a volume DBD with a discharge gap optimized to focus the discharge filament solely onto the seed surface. We demonstrated that this approach effectively modifies the surface without compromising the seed's internal integrity. Surface analysis revealed a significant oxygen enrichment, accompanied by a depletion of surface carbon (C-C/C-H bonds), a pattern regularly observed in atmospheric plasma treatment of seeds. These changes from a hydrophobic, hydrocarbon-dominated surface to a polar, oxygen-enriched, hydrophilic surface were corroborated using the sessile drop method. It revealed a sudden increase in the polar component of surface energy following plasma treatment, demonstrating that atmospheric plasma treatment converts the initially hydrophobic, hydrocarbon-dominated barley seed surface into a polar, chemically heterogeneous interface enriched in oxygen- and nitrogen-containing functionalities, while simultaneously reducing the total surface carbon content. The resulting functionalization is highly relevant for downstream biological effects, such as enhanced wettability, faster imbibition, and potentially the modulation of early germination phases.

The imbibition results confirm that plasma treatment improves water absorption in kernels, with the best case resulting in an almost 10% increase compared to the untreated reference sample. However, the non-monotonic nature of imbibition with plasma treatment duration (in contrast to the monotonic change in surface chemistry) reveals a deeper dynamic of water absorption and distribution in kernels beyond simple surface hydrophilicity and highlights the critical importance of plasma dose optimization to avoid loss of beneficial surface chemistry by overtreatment. This was mainly observed in the decrease in root length when the variant was treated for 300 s, which showed a nearly 30% decrease compared to the other variants. However, the germination tests showed no statistically significant effect of plasma on the germination of treated dry barley seeds, despite their faster imbibition.

In conclusion, this research highlights the potential of Volume DBD plasma as a technique that fulfills one of the basic prerequisites for successful barley seed priming, accelerated seed imbibition. We demonstrated that brief direct exposure induces oxygen-rich surface functionalization, facilitating rapid water uptake. Further optimization of the method is necessary to meet additional requirements, such as accelerated, synchronized germination and emergence, uniform sprout development, increased seedling vigor, and enhanced stress tolerance. A carefully developed and applied approach to determining plasma dose during exposure will hopefully allow us to reveal causal relationships in the biological response of treated seeds to changes in treatment parameters and plasma properties (e.g., when switching from plasma produced in synthetic air to plasma produced in humid air). In this context, a study of barley seed treatment under humid air conditions (which produce other chemically reactive species, such as hydroxyl radical or hydrogen peroxide) is currently underway. Moving forward, scaling this technology for industrial-scale seed processing/priming might be a critical step in future-proofing global grain production.

Author contributions

Conceptualization: Šimek; methodology: Prukner; software: Arora, Prukner; validation: Fujera, Širůčková Lónová; formal analysis: Homola, Kalousek; investigation: Fujera, Širůčková Lónová, Artemenko; resources: Prukner, Homola, Artemenko; data curation: Fujera, Širůčková Lónová; writing—original draft preparation: Fujera, Homola, Širůčková Lónová; writing—review and editing: Homola, Šimek, Kalousek; visualization: Fujera, Širůčková Lónová; supervision: Šimek, Homola. All authors have read and agreed to the published version of the manuscript.

Conflicts of interest

The authors declare no conflicts of interest.

Data availability

The additional data are provided as part of the Supplementary Information. The remaining raw data will be made available by the authors upon request.

Acknowledgements

T.H. acknowledges LM2023039, funded by the Ministry of Education, Youth and Sports of the Czech Republic, and A.A. acknowledges the support of project LM2023051 (research infrastructure of CzechNanoLab).

Notes and references

Open Access Article. Published on 15 June 2026. Downloaded on 6/15/2026 11:33:03 PM. This article is licensed under a Creative Commons Attribution 3.0 Unported Licence.

Sustainable Food Technology Accepted Manuscript

1 D. Knorr, A. Froehling, H. Jaeger, K. Reineke, O. Schlueter and K. Schoessler, *Annu. Rev. Food Sci. Technol.*, 2011, **2**, 203–235.

2 C. Sarangapani, A. Patange, P. Bourke, K. Keener and P. J. Cullen, *Annu. Rev. Food Sci. Technol.*, 2018, **9**, 609–629.

3 R. Brandenburg, A. Bogaerts, W. Bongers, A. Fridman, G. Fridman, B. R. Locke, V. Miller, S. Reuter, M. Schiorlin, T. Verreycken and K. (Ken) Ostrikov, *Plasma Processes and Polymers*, 2019, **16**, 1700238.

4 P. Attri, K. Ishikawa, T. Okumura, K. Koga and M. Shiratani, *Processes 2020, Vol. 8, Page 1002*, 2020, **8**, 1002.

5 M. Šimek and T. Homola, *The European Physical Journal D*, 2021, **75**, 210.

6 P. Ranieri, N. Sponsel, J. Kizer, M. Rojas-Pierce, R. Hernández, L. Gatiboni, A. Grunden and K. Stapelmann, *Plasma Processes and Polymers*, 2021, **18**, 2000162.

7 P. Pal, H. Sehgal, M. Joshi, G. Arora, M. Simek, R. P. Lamba, S. Maurya and U. N. Pal, *Planta 2025 261:5*, 2025, **261**, 109-.

8 F. Bilea, M. Garcia-vaquero, M. Magureanu, I. Mihaila, M. Mozetič, J. Pawłat, G. Primc, N. Puač, A. Stancampiano, I. Topala, R. Žūkienė, F. Bilea, M. Garcia-vaquero, M. Magureanu, I. Mihaila, V. Mildažienė, M. Mozetič, J. Pawłat, G. Primc, N. Puač, E. Robert, F. Bilea, M. Garcia-vaquero, M. Magureanu and I. Mihaila, *CRC. Crit. Rev. Plant Sci.*, 2024, **0**, 1–59.

9 A. Waskow, J. Betschart, D. Butscher, G. Oberbossel, D. Klöti, A. Büttner-Mainik, J. Adamcik, P. R. von Rohr and M. Schuppler, *Front. Microbiol.*, 2018, **9**, 414127.

10 A. Waskow, A. Howling and I. Furno, *Front. Phys.*, 2021, **9**, 617345.

11 P. F. Ambrico, M. Šimek, C. Rotolo, M. Morano, A. Minafra, M. Ambrico, S. Pollastro, D. Gerin, F. Faretra and R. M. De Miccolis Angelini, *Sci. Rep.*, 2020, **10**, 3673.

12 P. F. Ambrico, M. Šimek, M. Ambrico, M. Morano, V. Prukner, A. Minafra, I. Allegretta, C. Porfido, G. S. Senesi and R. Terzano, *J. Phys. D Appl. Phys.*, DOI:10.1088/1361-6463/ab5b1b.

13 T. Kalachova, B. Jindřichová, R. Pospíchalová, J. Fujera, A. Artemenko, J. Jančík, A. Antonova, O. Kylián, V. Prukner, L. Burketová, M. Šimek and T. Homola, *J. Agric. Food Chem.*, 2024, **72**, 5609–5624.

14 A. Shelar, A. V. Singh, P. Dietrich, R. S. Maharjan, A. Thissen, P. N. Didwal, M. Shinde, P. Laux, A. Luch, V. Mathe, T. Jahnke, M. Chaskar and R. Patil, *RSC Adv.*, 2022, **12**, 10467–10488.

15 C. E. Luchian, C. Lungoci, M.-A. Ciolan, C.-M. Rimbu, L. D. Miron and I. Motrescu, *Applied Sciences 2025, Vol. 15, Page 10366*, 2025, **15**, 10366.

16 E. Jankaitytė, Z. Naučienė, L. Degutytė-Fomins, A. Judickaitė, R. Žūkienė, I. Januškaitienė, G. Kudirka, K. Koga, M. Shiratani and V. Mildažienė, *Agronomy 2025, Vol. 15, Page 1371*, 2025, **15**, 1371.

17 M. Dhayal, S.-Y. Lee and S.-U. Park, *Vacuum*, 2006, **80**, 499–506.

18 L. Ling, L. Jiangang, S. Minchong, Z. Chunlei and D. Yuanhua, *Sci. Rep.*, 2015, **5**, 13033.

19 B. Adhikari, M. Adhikari, B. Ghimire, B. C. Adhikari, G. Park and E. H. Choi, *Free Radic. Biol. Med.*, 2020, **156**, 57–69.

20 D. N. Abeysingha, S. Dinesh, S. M. Kottage, L. Chen, M. S. Roopesh and M. S. Thilakarathna, *PLoS One*, 2025, **20**, e0322108.

21 L. Ling, J. Jiafeng, L. Jiangang, S. Minchong, H. Xin, S. Hanliang and D. Yuanhua, *Sci. Rep.*, 2014, **4**, 5859.

22 L. Geng, M. Li, G. Zhang and L. Ye, *Food Quality and Safety*, 2022, **6**, 1–13.

23 J. Lukinac and M. Jukić, *Plants*, 2022, **11**, 3519.

24 H. Rani and R. D. Bhardwaj, *J. Food Sci.*, 2021, **86**, 3322–3340.

25 T. Evers and S. Millar, *J. Cereal Sci.*, 2002, **36**, 261–284.

26 M. V. Rodríguez, J. M. Barrero, F. Corbineau, F. Gubler and R. L. Benech-Arnold, *Seed Sci. Res.*, 2015, **25**, 99–119.

27 K. R. Grant, M. Brennan and S. P. Hoad, *Front. Plant Sci.*, 2021, **11**, 614334.

28 Z. Ma, N. V. Bykova and A. U. Igamberdiev, *Crop J.*, 2017, **5**, 459–477.

29 K. Weitbrecht, K. Müller and G. Leubner-Metzger, *J. Exp. Bot.*, 2011, **62**, 3289–3309.

30 M. Brennan, T. Shepherd, S. Mitchell, C. F. E. Topp and S. P. Hoad, *BMC Plant Biol.*, 2017, **17**, 169-.

31 D. Chachalis and M. L. Smith, *Seed Science and Technology*, 2000, **28**, 321–331.

32 Woodstock L. W., *Journal of Seed Technology*, 1988, **12**, 1–15.

View Article Online
DOI: 10.1039/D6FB00081A

Open Access Article. Published on 15 June 2026. Downloaded on 6/15/2026 11:33:03 PM. This article is licensed under a Creative Commons Attribution 3.0 Unported Licence.

Sustainable Food Technology Accepted Manuscript

This journal is © The Royal Society of Chemistry 20xx

Please do not adjust margins

View Article Online
DOI: 10.1039/D5FB00091A

33 N. Neitzel, M. Eder, R. Hosseinpourpia, T. Walther and S. Adamopoulos, *Mater. Today Commun.*, 2023, **36**, 106602.

34 J. Graça, *Front. Chem.*, 2015, **3**, 163798.

35 E. I. Evstigneyev and S. M. Shevchenko, *Wood Sci. Technol.*, 2019, **53**, 7–47.

36 L. A. Del Río, *J. Exp. Bot.*, 2015, **66**, 2827–2837.

37 M. Caliskan and A. C. Cuming, *Plant Journal*, 1998, **15**, 165–171.

38 Z. Ma, F. Marsolais, N. V. Bykova and A. U. Igamberdiev, *Front. Plant Sci.*, 2016, **7**, 179637.

39 Z. Ma, F. Marsolais, M. A. Bernards, M. W. Sumarah, N. V. Bykova and A. U. Igamberdiev, *Plant Science*, 2016, **248**, 37–44.

40 P. R. Rotondo, D. Aceto, M. Ambrico, A. M. Stellacci, F. Faretra, R. M. De Miccolis Angelini and P. F. Ambrico, *Sci. Rep.*, 2025, **15**, 5536.

41 P. R. Rotondo, D. Aceto, C. Rotolo, M. Ambrico, G. Dilecce, F. Faretra, R. M. De Miccolis Angelini and P. F. Ambrico, *Plasma Chemistry and Plasma Processing*, 2023, **43**, 1819–1842.

42 P. F. Ambrico, M. Šimek, M. Morano, R. M. De Miccolis Angelini, A. Minafra, P. Trotti, M. Ambrico, V. Prukner and F. Faretra, *J. Phys. D Appl. Phys.*, 2017, **50**, 305401.

43 T. Homola, V. Prukner, A. Artemenko, J. Hanuš, O. Kylián and M. Šimek, *J. Appl. Phys.*, DOI:10.1063/5.0039165.

44 P. R. Rotondo, C. Rotolo, P. Hoffer, J. Fujera, V. Prukner, F. Faretra, R. M. De Miccolis Angelini and M. Šimek, *Scientific Reports 2025 15:1*, 2025, **15**, 28106-.

45 J. Fujera, P. Hoffer, V. Prukner and M. Šimek, *Plasma*, 2025, **8**, 11.

46 A. Waskow, F. Avino, A. Howling and I. Furno, *Plasma Processes and Polymers*, 2022, **19**, 2100152.

47 A. Perea-Brenes, A. Gómez-Ramírez, C. López-Santos, M. Oliva-Ramírez, R. Molina, J. Cotrino, J. L. García, M. Cantos and A. R. González-Elipe, *Plasma Processes and Polymers*, DOI:10.1002/ppap.202200035.

48 D. K. Owens and R. C. Wendt, *Estimation of the Surface Free Energy of Polymers*, 1969, vol. 13.

49 R. J. Good, *J. Adhes. Sci. Technol.*, 1992, **6**, 1269–1302.

50 P. Svačina, *Czech Journal of Genetics and Plant Breeding*, 2002, **38**, 139–140.

51 B. Šerá, in *Sborník recenzovaných vědeckých prací 2019*, Česká zemědělská univerzita v Praze, Prague, 2019, vol. 9, pp. 147–152.

52 J. H. T. Barros, U. M. Sampaio, F. M. Montenegro, C. J. Steel, J. de Amorim Filho and M. T. P. S. Clerici, *Research, Society and Development*, 2022, **11**, e15611326261.

53 S. Srisonphan, N. Tephiruk, S. Homkanchan, J. Puttha, S. Suwannarat and N. Teerakawanich, *Results in Engineering*, 2025, **26**, 105434.

54 S. Srisonphan and V. Kasemsuwan, *Surfaces and Interfaces*, 2021, **22**, 100877.

55 S. Srisonphan, K. Ruangwong and C. Thammaniphit, *Plasma Chemistry and Plasma Processing*, 2020, **40**, 1253–1265.

56 Manley T. C., *Transactions of The Electrochemical Society*, 1943, **84**, 83.

57 T. Homola, V. Prukner, P. Hoffer and M. Šimek, *Plasma Sources Sci. Technol.*, 2020, **29**, 095014.

58 A. V. Pipa, J. Koskulics, R. Brandenburg and T. Hoder, *Review of Scientific Instruments*, 2012, **83**, 115112.

59 M. Markowski, K. Majewska, D. Kwiatkowski, M. Malkowski and G. Burdylo, *Int. J. Food Prop.*, 2010, **13**, 890–903.

60 V. Guerra, A. Tejero-del-Caz, C. D. Pintassilgo, M. Šimek and Z. Bonaventura, *J. Phys. D Appl. Phys.*, 2018, **51**, 504004.

61 M. Šimek, *J. Phys. D Appl. Phys.*, 2014, **47**, 463001.

62 G. Scott, A. Almasrahi, F. Malekpoor Mansoorkhani, M. Rupar, M. Dickinson and G. Shama, *Plant Pathol.*, 2019, **68**, 700–707.

63 G. Ries, W. Heller, H. Puchta, H. Sandermann, H. K. Seldlitz and B. Hohn, *Nature 2000 406:6791*, 2000, **406**, 98–101.

64 J. F. Ma, A. Higashitani, K. Sato and K. Takeda, *Plant Soil*, 2003, **249**, 383–387.

65 S. N. Azizi, A. R. Dehnavi and A. Joorabdoozha, *Mater. Res. Bull.*, 2013, **48**, 1753–1759.

66 R. K. . Maiti, *Crop plant anatomy*, CABI, 2012.

67 S. Inanaga and A. Okasaka, *Soil Sci. Plant Nutr.*, 1995, **41**, 103–110.

68 S. Inanaga, A. Okasaka and S. Tanaka, *Soil Sci. Plant Nutr.*, 1995, **41**, 111–117.

Open Access Article. Published on 15 June 2026. Downloaded on 6/15/2026 11:33:03 PM.
This article is licensed under a Creative Commons Attribution 3.0 Unported Licence.

Sustainable Food Technology Accepted Manuscript

Please do not adjust margins

69 A. El Moukhtari, N. Lamsaadi, S. Lebreton, M. Mouradi, C. Cabassa, P. Carol, A. Savoure and M. Farissi, *Biologia (Bratisl).*, 2023, **78**, 1961–1977.

70 D. Ulfianida and D. Rachmawati, *BIO Web Conf.*, 2024, **94**, 06007.

71 M. Janmohammadi and N. Sabaghnia, *Bot. Lith.*, 2015, **21**, 13–21.

72 A. El Moukhtari, M. Ksiaa, W. Zorrig, C. Cabassa, C. Abdelly, M. Farissi and A. Savoure, *Journal of Plant Growth Regulation 2022 42:6*, 2022, **42**, 3323–3341.

73 R. Ben Youssef, N. Jelali, N. Boukari, A. Albacete, C. Martinez, F. P. Alfocea and C. Abdelly, *Plants 2021, Vol. 10, Page 2264*, 2021, **10**, 2264.

74 A. Gómez-Ramírez, C. López-Santos, M. Cantos, J. L. García, R. Molina, J. Cotrino, J. P. Espinós and A. R. González-Elipe, *Sci. Rep.*, DOI:10.1038/s41598-017-06164-5.

75 P. Šrámková, D. Kostoláni, S. Kyzek, M. Bathoova, S. Ďurčányová, M. Stupavská, E. Gálová, A. Zahoranová and R. Švubová, *Scientific Reports 2025 15:1*, 2025, **15**, 35001-.

76 A. Perea-Brenes, N. Ruiz-Pino, F. Yubero, J. L. Garcia, A. R. Gonzalez-Elipe, A. Gomez-Ramirez, A. Prados and C. Lopez-Santos, *J. Agric. Food Chem.*, 2025, **73**, 6486–6499.

77 B. Demri and D. Muster, *J. Mater. Process. Technol.*, 1995, **55**, 311–314.

78 J. Sharma, T. Gora, J. D. Rimstidt and R. Staley, *Chem. Phys. Lett.*, 1972, **15**, 232–235.

79 Y. L. Yan, M. A. Helfand and C. R. Clayton, *Appl. Surf. Sci.*, 1989, **37**, 395–405.

80 P. Šrámková, R. Švubová, D. Kostoláni, S. Kyzek, M. Bathoova, E. Gálová, S. Ďurčányová, M. Stupavská, D. Kováčik and A. Zahoranová, *Innovative Food Science & Emerging Technologies*, 2026, **107**, 104385.

81 J. Tomeková, R. Švubová, Slováková, Holubová-Čerevková, S. Kyzek, E. Gálová and A. Zahoranová, *Plasma Chemistry and Plasma Processing*, 2024, **44**, 487–507.

82 S. Ďurčányová, Ľ. Slováková, M. Klas, J. Tomeková, P. Ďurina, M. Stupavská, D. Kováčik and A. Zahoranová, *Plasma Chemistry and Plasma Processing*, 2023, **43**, 1863–1885.

83 Y. Shapira, V. Multanen, G. Whyman, Y. Bormashenko, G. Chaniel, Z. Barkay and E. Bormashenko, *Colloids Surf. B Biointerfaces*, 2017, **157**, 417–423.

84 A. Vesel, A. Macovei, A. Balestrazzi, S. A. Gupta Tondepu, C. Dueñas, V. Locato, T. C. Tonto, C. Zoani, D. Lojen, G. Primc, R. Zaplotnik, N. Ogrinc, M. Lehocky and M. Mozetič, *Appl. Surf. Sci.*, 2025, **691**, 162674.

85 T. Rongsangchaicharean, K. Ruangwong, D. Onwimol, N. Tephiruk, S. Suwannarat and S. Srisonphan, *J. Phys. D Appl. Phys.*, 2022, **55**, 365201.

86 N. Ahmed, K. S. Siow, M. F. M. R. Wee and A. Patra, *Scientific Reports 2023 13:1*, 2023, **13**, 1675-.

87 S. Murakonda and M. Dwivedi, *Biomass Convers. Biorefin.*, 2024, **14**, 28233–28251.

88 Y. Bao, L. Reddivari and J. Y. Huang, *LWT*, 2020, **133**, 109970.

89 D. Mehta, A. Purohit, P. Bajarh, K. Yadav, U. S. Shivhare and S. K. Yadav, *Innovative Food Science & Emerging Technologies*, 2022, **78**, 103027.

90 M. L. H. Gruwel, B. Chatson, X. S. Yin and S. Abrams, *Int. J. Food Sci. Technol.*, 2001, **36**, 161–168.

91 M. Koizumi, K. Kikuchi, S. Isobe, N. Ishida, S. Naito and H. Kano, *Ann. Bot.*, 2008, **102**, 343–352.

92 N. V Bykova, J. Hu, Z. Ma, A. U. Igamberdiev, N. V Bykova, J. Hu, Z. Ma and • A U Igamberdiev, 2015, 177–195.

93 Z. Ma, F. Marsolais, M. A. Bernards, M. W. Sumarah, N. V. Bykova and A. U. Igamberdiev, *Plant Science*, 2016, **248**, 37–44.

94 C. Bailly, H. El-Maarouf-Bouteau and F. Corbineau, *C. R. Biol.*, 2008, **331**, 806–814.

95 P. C. Bethke, in *Redox Metabolism and Longevity Relationships in Animals and Plants*, Taylor & Francis, 1st edn., 2009, pp. 37–50.

96 K. Dębska, U. Krasuska, K. Budnicka, R. Bogatek and A. Gniazdowska, *J. Plant Physiol.*, 2013, **170**, 480–488.

97 M. G. Mostofa, Md. M. Rahman, Md. M. U. Ansary, S. S. Keya, M. Abdelrahman, Md. G. Miah and L.-S. Phan Tran, *Crit. Rev. Biotechnol.*, 2021, **41**, 918–934.

98 Q. H. Pho, D. Losic, K. (Ken) Ostrikov, N. N. Tran and V. Hessel, *React. Chem. Eng.*, 2020, **5**, 1374–1396.

99 P. Attri, K. Ishikawa, T. Okumura, K. Koga, M. Shiratani and V. Mildaziene, *Sci. Rep.*, 2021, **11**, 2539.

View Article Online DOI: 10.1039/D5FB00084A

Sustainable Food Technology Accepted Manuscript

Open Access Article. Published on 15 June 2026. Downloaded on 6/15/2026 11:33:03 PM. This article is licensed under a Creative Commons Attribution 3.0 Unported Licence.

This journal is © The Royal Society of Chemistry 20xx

Please do not adjust margins

View Article Online
DOI: 10.1039/D6FB00081A

100 T. Okumura, T. Anan, H. Shi, P. Attri, K. Kamataki, N. Yamashita, N. Itagaki, M. Shiratani, Y. Ishibashi, K. Koga and V. Mildažienė, *Applied Physics Express*, 2024, **17**, 057001.

101 S. Park, B. Y. Choi, Y. bin Seol and J. Kim, *Free Radic. Res.*, 2025, **59**, 545–556.

Open Access Article. Published on 15 June 2026. Downloaded on 6/15/2026 11:33:03 PM.
This article is licensed under a Creative Commons Attribution 3.0 Unported Licence.

Sustainable Food Technology Accepted Manuscript

View Article Online
DOI: 10.1039/D6FB00081A

Data availability

The additional data are provided as part of the Supplementary Information. The remaining raw data will be made available by the authors upon request.

Open Access Article. Published on 15 June 2026. Downloaded on 6/15/2026 11:33:03 PM.
This article is licensed under a Creative Commons Attribution 3.0 Unported Licence.

Sustainable Food Technology Accepted Manuscript